

# A Fast Algorithm for Implementation of Some Minimum $L_2$ Distance Estimators and Their Application to Image Segmentation

Jiwoong Kim and Hira L. Koul

University of South Florida and Michigan State University

## Abstract

Minimum distance estimation methodology based on empirical distribution function has been popular due to its desirable properties including robustness. Even though the statistical literature is awash with the research on the minimum distance estimation, the most of it is confined to the theoretical findings: only few statisticians conducted research on the application of the method to real world problems. Through this paper, we extend the domain of application of this methodology to various applied fields by providing a solution to a rather challenging and complicated computational problem. The problem this paper tackles is an image segmentation which has been used in various fields. We propose a novel method based on the classical minimum distance estimation theory to solve the image segmentation problem. The performance of the proposed method is then further elevated by integrating it with the “segmenting-together” strategy.

## 1 Introduction

In a series of papers, Wolfowitz [11], [12], [13] proposed a minimum distance estimation method for estimating the underlying parameters in some parametric models. The distances used in this method are based on certain empirical processes. He showed that this method enables one to obtain consistent estimators under much weaker conditions than those required for the consistency of maximum likelihood estimators. Much later, Donoho and Liu [2], [3] argued that in the one and two sample location models the minimum distance estimators based on integrated square distances involving residual empirical distribution functions have some desirable finite sample properties and tend to be automatically robust against some contaminated models. Koul [7], [9], [8], [10] showed that in regression and autoregressive time series models, the analogs of these estimators of the underlying parameter is given in terms of certain weighted residual empirical processes. These estimators include least absolute deviation (LAD), analogs of Hodges-Lehmann (H-L) estimators and several other estimators that are robust against outliers in errors and asymptotically efficient at some error distributions. Kim [6] showed that this method of estimation can also be applied to a linear regression model with weakly dependent errors and empirically demonstrated the finite sample efficiency of some of these estimators.

Despite these desirable properties, application of the MD estimation methodology to the real world problems, however, stands in a nascent stage due to primarily the computational difficulty. Still, the merits of the methodology demonstrated by many statisticians in the past decades is strong prima facie evidence which motivates the method to be applied to other problems. In this paper we apply this methodology to image segmentation problems with the hope it will yield better inference in these problems.

One caveat against using the this MD estimation method for solving the proposed image segmentation problem involves its computational complexity. One critical issue that causes this complexity for these estimators is illustrated in the next section. Naive application of the existing optimization numerical methods to minimize an integrated square difference of weighted residual empirical processes lead to a heavy and slow computation. Rather than resorting to them, we consummately investigate the structure of the distance function and exploit some of its useful characteristics to expedite computation. To that end, we propose a novel algorithm to enable the application of this MD method to the segmentation problem for the first time.

## 2 Minimum distance estimators

In this section we discuss a regression model used in segmented image analysis, a MD estimator of the underlying parameters in the model and a fast computational algorithm. To be more precise we begin with some definitions and a model for image segmentation.

**Definition 2.1** *In digital imaging, a **pixel** is a physical point in a raster image. A collection of  $MN$  pixels is denoted by*

$$S = \{(i, j) : 1 \leq i \leq M, 1 \leq j \leq N\}.$$

where  $M$  and  $N$  are known positive integers.

An image,  $Img$ , is a map from  $S$  to real line  $\mathbb{R}$ , which is expressed as an  $M \times N$  matrix

$$Img := \begin{bmatrix} g(1, 1) & g(1, 2) & \cdots & g(1, N) \\ g(2, 1) & \cdots & \cdots & g(2, N) \\ \vdots & \vdots & \vdots & \vdots \\ g(M, 1) & \cdots & \cdots & g(M, N) \end{bmatrix}$$

where  $g : \mathbb{R}^2 \rightarrow \mathbb{R}^D$  and  $g(i, j)$  denote the value of the image at the  $(i, j)$ th pixel. Clearly,  $Img = g(S)$ . Here,  $D$  denotes the number of channel. If  $D = 1$ , the resultant output is a grayscale image while a color image that we commonly see corresponds to the case of  $D = 3$ .

This study considers grayscale images, i.e.,  $D = 1$ . Pixel values of the grayscale images represent the contrast which ranges from the darkest (black) to the brightest (white).

Let  $K$  be a positive integer and  $S_k^{True}$ ,  $1 \leq k \leq K$  denote a partition of  $S$  so that  $S_i^{True} \cap S_j^{True} = \emptyset$  for  $i \neq j$  and

$$\bigcup_{k=1}^K S_k^{True} = S.$$

Let  $n_k$  and  $n$  denote cardinalities of  $S_k^{True}$  and  $S$ , respectively. Note that  $n = \sum_{k=1}^K n_k = MN$ . Subsequently, we write

$$S_k^{True} = \{(x_{ik}, y_{ik}), i = 1, 2, \dots, n_k : 1 \leq x_{ik} \leq M, 1 \leq y_{ik} \leq N\},$$

so that the image  $Img$  can be segmented into  $K$  sub-images:  $g(S_1^{True})$ ,  $g(S_2^{True})$ , ...,  $g(S_K^{True})$ .

For  $1 \leq i \leq n_k$  and  $k = 1, \dots, K$ , let

$$g(x_{ik}, y_{ik}) = p_k, \quad \text{if } (x_{ik}, y_{ik}) \in S_k^{True},$$

where  $0 \leq p_k \leq 1$ ; black and white pixels take the value of 0 and 1, respectively, while a gray pixel takes a value between 0 and 1.

For  $1 \leq i \leq n_k$  and  $k = 1, \dots, K$ , define  $\tilde{g} : \mathbb{R}^2 \rightarrow \mathbb{R}$  by the following relations

$$(2.1) \quad \tilde{g}(x_{ik}, y_{ik}) := g(x_{ik}, y_{ik}) + \varepsilon_i,$$

where  $\varepsilon_i$ 's are some random variables (r.v.'s). In the literature,  $\varepsilon_i$  is called "noise" since it blurs the true pixel value  $g(x_{ik}, y_{ik})$ . We shall assume  $\varepsilon_i$  to be independent and identically distributed (i.i.d.), having a continuous distribution symmetric around zero. We do not assume the knowledge of this distribution.

The image segmentation problem is to estimate  $S_1^{True}$ ,  $S_2^{True}$ , ...,  $S_K^{True}$  when we observe  $\tilde{g}(S)$  instead of  $g(S)$  under the presence of the noise. For the sake of brevity, let  $\mathbf{s}_{ik}$  denote  $i$ th pixel of  $S_k$ , that is,  $\mathbf{s}_{ik} := (x_{ik}, y_{ik})$ ,  $k = 1, \dots, K$ , in the sequel.

**Example 1.** Consider  $K = 2$ . Figure 1 describes images with and without a noise which is generated from the normal distribution with mean 0 and standard deviation 0.1. The set  $S$  will be the entire rectangle, while  $S_1^{True}$  is a white circle, and  $S_2^{True}$  is its complement. The values of a pixel belonging to  $S_1^{True}$  and  $S_2^{True}$  are 1 and 0, respectively. Hence,

$$g(\mathbf{s}_i) = \begin{cases} 1, & \text{if } \mathbf{s}_i \in S_1^{True}; \\ 0, & \text{if } \mathbf{s}_i \in S_2^{True}. \end{cases}$$

Or equivalently,  $g(\mathbf{s}_{i1}) = 1$ ,  $g(\mathbf{s}_{i2}) = 0$ , for all  $i$ . Note that the image will become more blurred when stronger noise is present, and hence segmentation of the white circle will be more challenging.



Figure 1: Images with and without a noise.

Next, we shall define the distance function. Let

$$\mathcal{S}^K = \{(S_1, S_2, \dots, S_K) : \cup_{i=1}^K S_i = S, S_i \cap S_j = \emptyset \text{ for all } i \neq j\}.$$

Note that any  $\mathbf{S} \in \mathcal{S}^K$  will be then a  $K$ -tuple whose elements are collections of pixels and partition  $S$  in an exhaustive and exclusive manner. Consider  $K = 5$ : see, e.g., Figure 9 which instantiates this case. The bottom in Figure 9 shows an  $4 \times 5$  image of 20 pixels of  $K(= 5)$  different colors: black, dark gray, gray, light gray, and white. Let  $S_i$  denote the collection of pixels of the  $i$ th color. For example,  $S_5 = \{(1, 5), (2, 4), (3, 2), (4, 4)\}$  is a collection of white pixels while  $S_1 = \{(1, 3), (2, 1), (3, 4), (4, 5)\}$  is composed of black pixels. Note that  $\mathbf{S} = (S_1, \dots, S_5) \in \mathcal{S}^5$  is a tuple of 5 exclusive and exhaustive partitions of  $S$ , the collection of entire pixels. Another example arises if we partition  $S$  by its column (not a color). Let  $\tilde{S}_i$  denote a collection of the pixels of the  $i$ th column of the image, then  $\tilde{S}_i = \{(k, i) : 1 \leq k \leq 4\}$ . Then  $\tilde{\mathbf{S}} = (\tilde{S}_1, \dots, \tilde{S}_5) \in \mathcal{S}^5$  is another tuple of 5 exclusive and exhaustive partitions of  $S$ .

Accordingly, define

$$\mathcal{L}(\mathbf{S}) = \int \sum_{k=1}^K \left[ \sum_{s_i \in S_k} \frac{1}{n_k} \left\{ \mathbf{I}(\tilde{g}(s_i) - p_k \leq x) - \mathbf{I}(-\tilde{g}(s_i) + p_k < x) \right\} \right]^2 dH(x),$$

for any  $\mathbf{S} = (S_1, \dots, S_K) \in \mathcal{S}^K$ , where  $n_k$ ,  $1 \leq k \leq K$  is the cardinality of  $S_k$ ,  $\mathbf{I}(\cdot)$  is an indicator function, and  $H$  is a nondecreasing right continuous function on  $\mathbb{R}$  to  $\mathbb{R}$  having left limits. The above class of distances, one for each  $H$ , is deduced from Koul [10] which deals with parametric linear and nonlinear regression and autoregressive models.

The image segmentation problem in terms of the above distance is the same as solving the minimization problem

$$\hat{\mathbf{S}} = \operatorname{argmin}_{\mathbf{S} \in \mathcal{S}^K} \mathcal{L}(\mathbf{S}),$$

where  $\hat{\mathbf{S}} = (\hat{S}_1, \dots, \hat{S}_K)$ .

Before proceeding further, we need the following assumptions on  $\varepsilon_i$  and the integrating measure  $H$ . Let  $F$  denote distribution function of  $\varepsilon_i$  assumed to be continuous and  $\varepsilon$  denote a r.v. having the same distribution as  $\varepsilon_1$ .

(a.1)  $\varepsilon_i$ 's are independently and identically distributed (i.i.d.) according to  $F$ .

(a.2)  $F$  is continuous and symmetric around zero, that is,  $F(-x) = 1 - F(x)$  for all  $x \in \mathbb{R}$ .

(a.3) The integrating measure  $H$  is  $\sigma$ -finite and symmetric around 0, i.e.,  $dH(-x) \equiv -dH(x)$ , and

$$\int_0^\infty (1 - F) dH < \infty.$$

**Remark 2.1** In the context of parametric linear regression model, the asymptotic normality of a large class of the analogs of the above minimum distance estimators is proved in Koul [10]. For a given  $F$  satisfying the given assumptions, it is possible find an  $H$  for which the corresponding m.d. estimator is asymptotically efficient. For example, if  $F$  is double exponential then  $H(x) \equiv \delta_0(x)$  – the d.f. degenerate at zero – yields an asymptotically efficient m.d. estimator while for logistic  $F$ ,  $H(x) \equiv x$  gives an asymptotically efficient m.d. estimator. At the same time both of these estimators are known to be robust against the gross errors.

Consider  $K = 2$  and  $H(x) \equiv x$ . Note that

$$(2.2) \quad \mathcal{L}(S_1, S_2) = \frac{1}{n_1^2} \int \left[ \sum_{s_i \in S_1} \left\{ \mathbf{I}(\tilde{g}(s_i) - p_1 \leq x) - \mathbf{I}(-\tilde{g}(s_i) + p_1 < x) \right\} \right]^2 dx \\ + \frac{1}{n_2^2} \int \left[ \sum_{s_j \in S_2} \left\{ \mathbf{I}(\tilde{g}(s_j) - p_2 \leq x) - \mathbf{I}(-\tilde{g}(s_j) + p_2 < x) \right\} \right]^2 dx,$$

where  $S_1 \cup S_2 = S$  and  $S_1 \cap S_2 = \emptyset$  while  $n_1$  and  $n_2$  denote the cardinality of  $S_1$  and  $S_2$ , respectively. Define the MD estimator  $(\hat{S}_1, \hat{S}_2)$  as

$$(2.3) \quad \mathcal{L}(\hat{S}_1, \hat{S}_2) = \inf_{(S_1, S_2) \in \mathcal{S}^2} \mathcal{L}(S_1, S_2).$$

**Theorem 2.1**  $\mathcal{L}$  is bounded in probability, that is, for all  $\eta > 0$  there is a  $0 < B_\eta < \infty$  such that

$$(2.4) \quad P(\mathcal{L}(S_1, S_2) \leq B_\eta) \geq 1 - \eta, \quad \forall (S_1, S_2) \in \mathcal{S}^2, \quad \forall n \geq 1.$$

Moreover, solutions to the optimization problem in (2.3) exist almost surely.

**Proof.** Arguing as in Koul (2002, Section 5.3), (2.2) can be simplified to

$$(2.5) \quad \mathcal{L}(S_1, S_2) = \frac{1}{n_1^2} \sum_{\mathbf{s}_i \in S_1} \sum_{\mathbf{s}_j \in S_1} f_{ij}^1 + \frac{1}{n_2^2} \sum_{\mathbf{s}_i \in S_2} \sum_{\mathbf{s}_j \in S_2} f_{ij}^2,$$

where

$$\begin{aligned} f_{ij}^1 &= |\tilde{g}(\mathbf{s}_i) + \tilde{g}(\mathbf{s}_j) - 2p_1| - |\tilde{g}(\mathbf{s}_i) - \tilde{g}(\mathbf{s}_j)|, \\ f_{ij}^2 &= |\tilde{g}(\mathbf{s}_i) + \tilde{g}(\mathbf{s}_j) - 2p_2| - |\tilde{g}(\mathbf{s}_i) - \tilde{g}(\mathbf{s}_j)|. \end{aligned}$$

Therefore,

$$\begin{aligned} E|\mathcal{L}(S_1, S_2)| &\leq \frac{1}{n_1^2} \sum_{\mathbf{s}_i \in S_1} \sum_{\mathbf{s}_j \in S_1} E[|\varepsilon_i + \varepsilon_j| + |\varepsilon_i - \varepsilon_j|] \\ &\quad + \frac{1}{n_2^2} \sum_{\mathbf{s}_i \in S_2} \sum_{\mathbf{s}_j \in S_2} E[|\varepsilon_i + \varepsilon_j| + |\varepsilon_i - \varepsilon_j|] \leq 4E|\varepsilon| < \infty. \end{aligned}$$

This fact and the Markov inequality readily imply the claim (2.4). Since  $\mathcal{S}^2$  is a finite set whose cardinality is  $2^{n_1+n_2}$ , any bounded function on it should have a minimum, thereby completing the proof of the theorem.  $\square$

Without the loss of any generality, in the sequel, the first argument  $S_1$  of the distance function  $\mathcal{L}(S_1, S_2)$  is used for brighter pixels of an image while the second argument  $S_2$  corresponds to the rest of the image as in Example 1.

Note that a solution to the optimization problem (2.3) does not have any closed-form expression, and hence, we seek a solution through numerical optimization. To that end, we start with a pair of randomly-selected pixels  $(S_1^{(0)}, S_2^{(0)})$  in the initial stage, find a better pair of collections  $(S_1^{(1)}, S_2^{(1)})$  which yields smaller value of  $\mathcal{L}$  than the values at the previous stage, and keep iterating this procedure until the convergence. Then, how can we select a better pair of collections? To answer this question, we introduce a concept of ‘‘a netgain’’ which is a quintessential part of our proposed method. For some pixel  $\mathbf{s} \in S_i$ , let  $S_i^{(-\{\mathbf{s}\})}$  and  $S_i^{(+\{\mathbf{s}\})}$  denote  $S_i \setminus \{\mathbf{s}\}$  and  $S_i \cup \{\mathbf{s}\}$ , respectively.

**Definition 2.2** Consider a pixel  $\mathbf{s}_i \in S_1$ . Then a netgain of  $\mathbf{s}_i$  is defined as

$$NG(\mathbf{s}_i; S_1) := \mathcal{L}(S_1^{(-\{\mathbf{s}_i\})}, S_2^{(+\{\mathbf{s}_i\})}) - \mathcal{L}(S_1, S_2),$$

which is a difference between the two distance functions consequential upon transferring  $\mathbf{s}_i$  from  $S_1$  to  $S_2$ . Similarly, a netgain of  $\mathbf{s}_j \in S_2$  is defined as

$$NG(\mathbf{s}_j; S_2) := \mathcal{L}(S_1^{(+\{\mathbf{s}_j\})}, S_2^{(-\{\mathbf{s}_j\})}) - \mathcal{L}(S_1, S_2).$$

Consider  $\mathbf{s}_k \in S_i$ . Recall that  $S_i^{(-\{\mathbf{s}_k\})}$  and  $S_j^{(+\{\mathbf{s}_k\})}$  are  $S_i \setminus \{\mathbf{s}_k\}$  and  $S_j \cup \{\mathbf{s}_k\}$ , respectively. For the sake of brevity, let  $S_i^{(-k)}$  and  $S_j^{(+k)}$  denote these two sets, respectively. Analogously, for  $\mathbf{s}_k, \mathbf{s}_h \in S_i$ ,  $S_i^{(-k,h)}$  and  $S_j^{(+k,h)}$  will denote  $S_i / \{\mathbf{s}_k, \mathbf{s}_h\}$  and  $S_j \cup \{\mathbf{s}_k, \mathbf{s}_h\}$ , respectively. Recall  $f_{ij}^1$  and  $f_{ij}^2$  from the proof of Theorem 2.1. Note that

$$\sum_{s_i \in S_1} \sum_{s_j \in S_1} f_{ij}^1 = \sum_{s_i \in S_1^{(-k)}} \sum_{s_j \in S_1^{(-k)}} f_{ij}^1 + 2 \sum_{s_i \in S_1^{(-k)}} f_{ki}^1 + f_{kk}^1,$$

and

$$\sum_{s_i \in S_2} \sum_{s_j \in S_2} f_{ij}^2 = \sum_{s_i \in S_2^{(+k)}} \sum_{s_j \in S_2^{(+k)}} f_{ij}^2 - 2 \sum_{s_i \in S_2} f_{ki}^2 - f_{kk}^2.$$

Therefore,

$$\begin{aligned} (2.6) \quad NG(\mathbf{s}_k; S_1) &= \mathcal{L}(S_1^{(-k)}, S_2^{(+k)}) - \mathcal{L}(S_1, S_2), \\ &= \left[ -\frac{2}{n_1^2} \sum_{s_i \in S_1} f_{ki}^1 + \frac{2}{n_2^2} \sum_{s_j \in S_2} f_{kj}^2 + \frac{1}{n_1^2} f_{kk}^1 + \frac{1}{n_2^2} f_{kk}^2 \right]. \end{aligned}$$

Note that  $NG(\mathbf{s}_k; S_1)$  is stochastically bounded, that is,  $NG(\mathbf{s}_k; S_1) = O_p(1)$ . Adoption of the concept of the netgain makes it convenient to analyze the distance function in that any difference between distance functions – one obtained from the original  $(S_1, S_2)$  and another obtained after several transfer of pixels from  $S_1$  to  $S_2$  – can be written as the sum of netgains of those pixels. For example, we have

$$\begin{aligned} \mathcal{L}(S_1^{(-k,h)}, S_2^{(+k,h)}) - \mathcal{L}(S_1, S_2) &= NG(\mathbf{s}_k; S_1) + NG(\mathbf{s}_h; S_1^{(-k)}), \\ &= NG(\mathbf{s}_h; S_1) + NG(\mathbf{s}_k; S_1^{(-h)}), \end{aligned}$$

for  $\mathbf{s}_k, \mathbf{s}_h \in S_1$ . Similarly,  $\mathbf{s}_k, \mathbf{s}_h \in S_2$ ,

$$\begin{aligned} \mathcal{L}(S_1^{(+k,h)}, S_2^{(-k,h)}) - \mathcal{L}(S_1, S_2) &= NG(\mathbf{s}_k; S_2) + NG(\mathbf{s}_h; S_2^{(-k)}), \\ &= NG(\mathbf{s}_h; S_2) + NG(\mathbf{s}_k; S_2^{(-h)}), \end{aligned}$$

when  $\mathbf{s}_k, \mathbf{s}_h \in S_2$ . For the general case, consider any  $S_1^{sub} \subset S_1$  where  $S_1^{sub} = \{\mathbf{u}_1, \mathbf{u}_2, \dots, \mathbf{u}_L\}$ . Then, we have

$$(2.7) \quad \mathcal{L}(S_1^{sub}, S \setminus S_1^{sub}) - \mathcal{L}(S_1, S_2) = NG(\mathbf{u}_1; S_1^{sub}) + \sum_{i=2}^L NG(\mathbf{u}_i; S_1^{sub} \setminus \cup_{j=1}^{i-1} \{\mathbf{u}_j\})$$

Define

$$\mathcal{NG}(S_1) := \{\mathbf{s}_i \in S_1 : NG(\mathbf{s}_i; S_1) < 0\}, \quad \mathcal{NG}(S_2) := \{\mathbf{s}_j \in S_2 : NG(\mathbf{s}_j; S_2) < 0\}.$$

As defined above,  $\mathcal{NG}(S_1)$  is a set of pixels which originally belong to  $S_1$ , and whose relocation to  $S_2$  will decrease the distance function.  $\mathcal{NG}(S_2)$  is defined similarly.

At this juncture, one important question arises: which pixels of  $S_1$  and  $S_2$  should be relocated to each other to decrease the distance function? Well, it is not unreasonable to consider pixels which belong to  $\mathcal{NG}(S_1)$  and  $\mathcal{NG}(S_2)$  as potential candidates. For the convenience of the further analysis, let  $\mathcal{NG}(S_1) := \{\mathbf{s}_1^1, \mathbf{s}_2^1, \dots, \mathbf{s}_{n_1}^1\}$  and  $\mathcal{NG}(S_2) := \{\mathbf{s}_1^2, \mathbf{s}_2^2, \dots, \mathbf{s}_{n_2}^2\}$ . Transferring all elements of  $\mathcal{NG}(S_1)$  from  $S_1$  to  $S_2$  will result in two new sets:  $S_1 \setminus \mathcal{NG}(S_1)$  and  $S_2 \cup \mathcal{NG}(S_1)$ . Then, difference between the consequential and initial distance functions can be written as

$$\mathcal{L}(S_1 \setminus \mathcal{NG}(S_1), S_2 \cup \mathcal{NG}(S_1)) - \mathcal{L}(S_1, S_2) = NG(\mathbf{s}_1^1; S_1) + \sum_{i=2}^{n_1} NG(\mathbf{s}_i^1; S_1 \setminus \cup_{j=1}^{i-1} \{\mathbf{s}_j^1\}).$$

It is worth noting the following facts; (1)  $\mathbf{s}_1^1 \in \mathcal{NG}(S_1)$  implies that the first term in the right-hand side of the above equation is less than 0, which means transfer of  $\mathbf{s}_1^1$  will always decrease the distance function; (2) the summand of the above equation  $NG(\mathbf{s}_i^1; S_1 \setminus \cup_{j=1}^{i-1} \{\mathbf{s}_j^1\})$  is not always negative even though  $NG(\mathbf{s}_i^1; S_1) < 0$ ; and (3) transfer of all  $\mathbf{s}_i^1$ 's in  $\mathcal{NG}(S_1)$  does not yield the greatest decrease of the distance function. To accomplish the desirable result, define  $\mathcal{T}(S_1) = \{\mathbf{t}_1, \mathbf{t}_2, \dots, \mathbf{t}_{n_*}\} \subset \mathcal{NG}(S_1)$  as follows:

$$\begin{aligned} \mathbf{t}_1 &:= \operatorname{argmin}_{\mathbf{s} \in \mathcal{NG}(S_1)} NG(\mathbf{s}; S_1), \\ \mathbf{t}_2 &:= \operatorname{argmin}_{\mathbf{s} \in \mathcal{NG}(S_1)} NG(\mathbf{s}; S_1 \setminus \{\mathbf{t}_1\}), \\ &\vdots \\ \mathbf{t}_{n_*} &= \operatorname{argmin}_{\mathbf{s} \in \mathcal{NG}(S_1)} NG(\mathbf{s}; S_1 \setminus \cup_{j=1}^{n_*-1} \{\mathbf{t}_j\}). \end{aligned}$$

To be more precise, we construct  $\mathcal{T}(S_1)$  as follows. Among the pixels of  $\mathcal{NG}(S_1)$ , find one which minimizes  $NG(\mathbf{s}; S_1)$ ; this pixel will be the first element of  $\mathcal{T}(S_1)$ , denoted by  $\mathbf{t}_1$ . Note that  $NG(\mathbf{t}_1; S_1) < 0$  by the definition of  $\mathcal{NG}(S_1)$ . Next, among the remaining pixels after removing  $\mathbf{t}_1$  from  $\mathcal{NG}(S_1)$ , find  $\mathbf{t}_2$  which minimizes  $NG(\mathbf{s}; S_1 \setminus \{\mathbf{t}_1\})$  and check a sign of the resulting netgain which plays a role as a stopping criterion. If  $NG(\mathbf{t}_2; S_1 \setminus \{\mathbf{t}_1\}) \geq 0$ , the construction of  $\mathcal{T}(S_1)$  will be halted; otherwise, we add it to  $\mathcal{T}(S_1)$  and proceed to find  $\mathbf{t}_3$ . Repeating this procedure until the stopping criterion is met will yield  $\mathcal{T}(S_1)$ .  $\mathcal{T}(S_2) \subset \mathcal{NG}(S_2)$  can be obtained in the same manner. By the way that  $\mathcal{T}(S_1)$  is constructed, we always have  $\mathcal{L}(S_1 \setminus \mathcal{T}(S_1), S_2 \cup \mathcal{T}(S_1)) < \mathcal{L}(S_1, S_2)$ . At the moment of trading some elements between  $S_1$  and  $S_2$ , we will, therefore, refer to  $\mathcal{T}(S_1)$  and  $\mathcal{T}(S_2)$  instead of  $\mathcal{NG}(S_1)$  and  $\mathcal{NG}(S_2)$ .

**Lemma 2.1** For  $\mathbf{s}_h, \mathbf{s}_k \in S_1$ ,  $\mathbf{s}_h \notin \mathcal{NG}(S_1)$ , that is,  $NG(\mathbf{s}_h; S_1) \geq 0$ , implies

$$\lim_{n \rightarrow \infty} P(NG(\mathbf{s}_h; S_1^{(-k)}) \geq 0) = 1,$$



and  $NG(\mathbf{s}_h; S_1^{(-k)}) \geq 0$  implies

$$\lim_{n \rightarrow \infty} P(NG(\mathbf{s}_h; S_1) \geq 0) = 1.$$

Similarly,  $\mathbf{s}_h \in \mathcal{NG}(S_1)$ , that is,  $NG(\mathbf{s}_h; S_1) < 0$ , implies

$$\lim_{n \rightarrow \infty} P(NG(\mathbf{s}_h; S_1^{(-k)}) < 0) = 1,$$

and  $NG(\mathbf{s}_h; S_1^{(-k)}) < 0$  implies

$$\lim_{n \rightarrow \infty} P(NG(\mathbf{s}_h; S_1) < 0) = 1.$$

**Remark 2.2** Lemma 2.1 shows that the probability of the same sign for  $NG(\mathbf{s}_h; S_1)$  and  $NG(\mathbf{s}_h; S_1^{(-k)})$  approaches to 1 as the number of pixels  $n$  increases. After selecting  $\mathbf{s}_1^1 \in \mathcal{NG}(S_1)$  to construct  $\mathcal{T}(S_1)$ , we will encounter a problem of a choice of another element of  $S_1$ . To that end, we checked elements of  $\mathcal{NG}(S_1)$  only. Lemma 2.1 shows that an element, say  $\mathbf{s}_h \in S_1$ , does not need to be considered for  $\mathcal{T}(S_1)$  if  $\mathbf{s}_h \notin \mathcal{NG}(S_1)$ . Note that the analogous result holds true for  $S_2$ . The proof for  $S_2$  is not included here since it is almost the same as one for  $S_1$ .

**Proof.** Note that  $\mathbf{s}_h \notin \mathcal{NG}(S_1)$  implies  $NG(\mathbf{s}_h; S_1) \geq 0$ . From (2.6), we have

$$NG(\mathbf{s}_h; S_1^{(-k)}) = NG(\mathbf{s}_h; S_1) + 2(f_{hk}^1/n_1^2 + f_{hk}^2/n_2^2).$$

It is easy to see that the second term in the above equation is  $o_p(1)$ . Thus, the claim follows from  $NG(\mathbf{s}_h; S_1) = O_p(1)$ .  $\square$

**Corollary 2.1** For  $\mathbf{s}_k, \mathbf{s}_h, \mathbf{s}_l \in S_1$ ,  $NG(\mathbf{s}_k; S_1) > NG(\mathbf{s}_h; S_1)$  implies

$$\lim_{n \rightarrow \infty} P(NG(\mathbf{s}_k; S_1^{(-l)}) > NG(\mathbf{s}_h; S_1^{(-l)})) = 1,$$

and  $NG(\tilde{\mathbf{s}}_k; S_1^{(-l)}) > NG(\mathbf{s}_h; S_1^{(-l)})$  implies

$$\lim_{n \rightarrow \infty} P(NG(\mathbf{s}_k; S_1) > NG(\mathbf{s}_h; S_1)) = 1.$$

**Proof.** From (2.6), the fact that both  $n^{-2}(f_{lk}^1 + f_{lk}^2)$  and  $n^{-2}(f_{lh}^1 + f_{lh}^2)$  are  $o_p(1)$  completes the proof of the claim.  $\square$

Starting with an initial pair of sets  $(S_1, S_2)$ , we compute  $\mathcal{T}(S_1)$  and transfer its elements to  $S_2$ ; let  $\tilde{S}_1 = S_1 \setminus \mathcal{T}(S_1)$  and  $\tilde{S}_2 = S_2 \cup \mathcal{T}(S_1)$ . Now we compute  $\mathcal{T}(\tilde{S}_2)$ , that is, we find  $\mathbf{s} \in \tilde{S}_2$  whose netgain is less than 0 and transfer of which to  $\tilde{S}_1$  will decrease the distance function. To that end, we will examine netgains of  $\mathbf{s}_i$ 's belonging  $\tilde{S}_2$ . When checking elements belonging to  $\tilde{S}_2$ , we may need to check original elements of  $S_2$  only, which seems quite rational. To put it another way, any elements of  $\mathcal{T}(S_1)$  may not be relocated back to  $S_1$  once they move to  $S_2$ . The justification for this argument is primarily based on the following lemma.

**Lemma 2.2** For any  $\mathbf{s}_k \in \mathcal{T}(S_1)$ ,  $NG(\mathbf{s}_k; \tilde{S}_2) > 0$ .

**Remark 2.3** Once some elements of  $S_1$  are transferred to  $S_2$ , they will not be relocated back to  $S_1$ . Lemma 2.2, therefore, conduces remarkable curtailment to the computational cost; otherwise their netgains should be redundantly computed, which is merely reinventing the wheel. This redundancy will incur cumbersome computation, especially in the initial stage of the computation when the cardinality of  $\mathcal{T}(S_1)$  is usually huge.

**Proof.** Assume that  $\mathcal{T}(S_1) = \{\mathbf{s}_1^1, \mathbf{s}_2^1, \dots, \mathbf{s}_h^1\}$ , that is,  $h$  elements of  $S_1$  are transferred to  $S_2$ . We will prove the case of  $h = 3$  only since the proof for the general case will be very similar, albeit not necessarily identical. We will prove the claim in reverse order of  $\mathbf{s}_i^1$ , thereby starting with checking a netgain of  $\mathbf{s}_3^1$  first and that of  $\mathbf{s}_1^1$  last. The reason for this is that the difficulty for the proof of the claim increases in the reverse order. Since we transfer  $\mathbf{s}_3^1$  last from  $S_1$  to  $S_2$ ,  $NG(\mathbf{s}_3^1; \tilde{S}_2)$  is simply equal to  $-NG(\mathbf{s}_3^1; S_1 \setminus \{\mathbf{s}_1^1, \mathbf{s}_2^1\})$  which is strictly positive; otherwise,  $\mathbf{s}_3^1 \notin \mathcal{T}(S_1)$  in that we do not transfer  $\mathbf{s}_3^1$  from  $S_1$  to  $S_2$  after  $\mathbf{s}_1^1$  and  $\mathbf{s}_2^1$  are transferred. Therefore, the claim for  $\mathbf{s}_3^1$  holds true. Next, consider  $\mathbf{s}_2^1$ . Observe that

$$\begin{aligned}
& NG(\mathbf{s}_2^1; \tilde{S}_2) \\
&= \mathcal{L}(S_1 \setminus \{\mathbf{s}_1, \mathbf{s}_3\}, S_2 \cup \{\mathbf{s}_1^1, \mathbf{s}_3^1\}) - \mathcal{L}(\tilde{S}_1, \tilde{S}_2) \\
&= \left[ \mathcal{L}(S_1 \setminus \{\mathbf{s}_1^1, \mathbf{s}_3^1\}, S_2 \cup \{\mathbf{s}_1^1, \mathbf{s}_3^1\}) - \mathcal{L}(S_1, S_2) \right] - \left[ \mathcal{L}(\tilde{S}_1, \tilde{S}_2) - \mathcal{L}(S_1, S_2) \right] \\
&= \left[ NG(\mathbf{s}_1^1; S_1) + NG(\mathbf{s}_3^1; S_1 \setminus \{\mathbf{s}_1^1\}) \right] - \left[ NG(\mathbf{s}_1^1; S_1) + NG(\mathbf{s}_2^1; S_1 \setminus \{\mathbf{s}_1^1\}) \right. \\
&\quad \left. + NG(\mathbf{s}_3^1; S_1 \setminus \{\mathbf{s}_1^1, \mathbf{s}_2^1\}) \right] \\
&= \left[ NG(\mathbf{s}_3^1; S_1 \setminus \{\mathbf{s}_1^1\}) - NG(\mathbf{s}_2^1; S_1 \setminus \{\mathbf{s}_1^1\}) \right] - NG(\mathbf{s}_3^1; S_1 \setminus \{\mathbf{s}_1^1, \mathbf{s}_2^1\}) \\
&\geq 0,
\end{aligned}$$

where the inequality follows from the way we constructed  $\mathcal{T}(S_1)$ , that is,  $NG(\mathbf{s}_2^1; S_1 \setminus \{\mathbf{s}_1^1\}) \leq NG(\mathbf{s}_3^1; S_1 \setminus \{\mathbf{s}_1^1\})$  and  $NG(\mathbf{s}_3^1; S_1 \setminus \{\mathbf{s}_1^1, \mathbf{s}_2^1\}) < 0$ . Finally, consider the claim for  $\{\mathbf{s}_1^1\}$ . Analogous to  $NG(\mathbf{s}_2^1; \tilde{S}_2)$ ,  $NG(\mathbf{s}_1^1; \tilde{S}_2)$  can be rewritten as

$$\begin{aligned}
NG(\mathbf{s}_1^1; \tilde{S}_2) &= \left[ NG(\mathbf{s}_2^1; S_1) - NG(\mathbf{s}_1^1; S_1) \right] + \left[ NG(\mathbf{s}_3^1; S_1 \setminus \{\mathbf{s}_2^1\}) - NG(\mathbf{s}_2^1; S_1 \setminus \{\mathbf{s}_3^1\}) \right] \\
&\quad - NG(\mathbf{s}_3^1; S_1 \setminus \{\mathbf{s}_1^1, \mathbf{s}_2^1\}).
\end{aligned}$$

The fact that the first and third terms of the right-hand side of the equation are positive again follows from the way  $\mathcal{T}(S_1)$  is constructed, which implies that the proof of the claim for  $\mathbf{s}_1^1$  – and the proof of the lemma – amounts to showing  $NG(\mathbf{s}_3^1; S_1 \setminus \{\mathbf{s}_2^1\}) \geq NG(\mathbf{s}_2^1; S_1 \setminus \{\mathbf{s}_3^1\})$ . Note that

$$\begin{aligned}
\mathcal{L}(S_1 \setminus \{\mathbf{s}_2^1, \mathbf{s}_3^1\}, S_2 \cup \{\mathbf{s}_2^1, \mathbf{s}_3^1\}) - \mathcal{L}(S_1, S_2) &= NG(\mathbf{s}_2^1; S_1) + NG(\mathbf{s}_3^1; S_1 \setminus \{\mathbf{s}_2^1\}), \\
&= NG(\mathbf{s}_3^1; S_1) + NG(\mathbf{s}_2^1; S_1 \setminus \{\mathbf{s}_3^1\}).
\end{aligned}$$

Therefore,

$$NG(\mathbf{s}_3^2; S_1 \setminus \{\mathbf{s}_2^1\}) - NG(\mathbf{s}_2^1; S_1 \setminus \{\mathbf{s}_3^1\}) = NG(\mathbf{s}_3^1; S_1) - NG(\mathbf{s}_2^1; S_1) \geq 0,$$

where the inequality, again, follows from Corollary 2.1 and the way  $\mathcal{T}(S_1)$  is constructed, that is,

$$NG(\mathbf{s}_2^1; S_1 \setminus \{\mathbf{s}_1^1\}) < NG(\mathbf{s}_3^1; S_1 \setminus \{\mathbf{s}_1^1\}),$$

thereby completing the proof of the lemma.  $\square$

Based on Lemma 2.2, we examine elements originally belonging to  $S_2$  only when constructing  $\mathcal{T}(\tilde{S}_2)$ , which implies  $\mathcal{T}(\tilde{S}_2) = \mathcal{T}(S_2)$ ; next we transfer all pixels of  $\mathcal{T}(S_2)$  from  $\tilde{S}_2$  to  $\tilde{S}_1$ . Finally, we have  $(S_1 \setminus \mathcal{T}(S_1)) \cup \mathcal{T}(S_2)$  and  $(S_2 \cup \mathcal{T}(S_1)) \setminus \mathcal{T}(S_2)$  in the end of the stage; update  $S_1$  and  $S_2$  with these two sets for the next stage. Then we repeat this procedure until we get  $\mathcal{T}(S_1) = \mathcal{T}(S_2) = \emptyset$ , i.e., there is no need to relocate elements between  $S_1$  and  $S_2$  to decrease the distance function. The proposed algorithm is summarized below.

---

**The proposed algorithm:**

---

Choose a random initial pair  $(S_1, S_2)$

Set  $\mathcal{T}_1 = \mathcal{T}_2 = \emptyset$

while  $\mathcal{T}_1 \neq \emptyset$  or  $\mathcal{T}_2 \neq \emptyset$

    compute  $\mathcal{T}_1 := \mathcal{T}(S_1)$  and  $\mathcal{T}_2 := \mathcal{T}(S_2)$ .

    transfer all pixels of  $\mathcal{T}_1$  from  $S_1$  to  $S_2$ .

    transfer all pixels of  $\mathcal{T}_2$  from  $S_2$  to  $S_1$ .

    update  $S_1$  and  $S_2$  to  $(S_1 \setminus \mathcal{T}_1) \cup \mathcal{T}_2$  and  $(S_2 \setminus \mathcal{T}_2) \cup \mathcal{T}_1$ , respectively

end while

Return  $S_1$  and  $S_2$

---

Let  $\Omega$  denote a collection of all subsets of  $S$ , that is,  $\Omega := \{A : A \subset S\}$ . We shall define a metric to measure a distance between any elements of  $\Omega$ . For  $A \in \Omega$ , let  $|A|$  denote its cardinality. For real numbers  $a, b \in \mathbb{R}$ , let  $a \vee b := \max(a, b)$ . Define a function  $\delta : \Omega \times \Omega \rightarrow \mathbb{N}$  where

$$\delta(A, B) = \begin{cases} ||A| - |B||, & \text{if } A \subset B \text{ or } B \subset A; \\ |A| \vee |B|, & \text{if } A \cap B = \emptyset; \\ (|A| - |A \cap B|) \vee (|B| - |A \cap B|), & \text{otherwise.} \end{cases}$$

Note that  $||A| - |B|| \leq (|A| - |A \cap B|) \vee (|B| - |A \cap B|) \leq |A| \vee |B|$  for all  $A, B \in \Omega$ , that is, a distance between  $A$  and  $B$  gets smaller as two sets share more in common. Also, we can see that  $||A| - |B||$  and  $|A| \vee |B|$  play as lower and upper bounds for  $\delta(A, B)$ .

**Lemma 2.3**  $\delta$  is a valid metric, that is, for  $A, B, C \in \Omega$ , the followings hold:

1.  $\delta(A, B) = 0 \Leftrightarrow A = B$ ,
2.  $\delta(A, B) = \delta(B, A)$ ,
3.  $\delta(A, B) \leq \delta(A, C) + \delta(C, B)$ .

**Proof.** Proofs of the first and second claims are trivial. For the last claim, assume  $|A| \geq |B|$ , i.e.  $|A| \vee |B| = |A|$ . Consider  $B \subset A$ . Then, we have

$$\delta(A, B) = ||A| - |B|| \leq (||A| - |C||) + (||B| - |C||) \leq \delta(A, C) + \delta(B, C),$$

where the first and second inequalities follow from the triangle inequality and the lower bound of  $\delta$ , respectively.

Now, consider  $A \cap B = \emptyset$ , which implies  $\delta(A, B) = |A|$ . For either  $C \subset A$  or  $C \subset B$ , the proof of the claim is straightforward. For  $A \cap C \neq \emptyset$  but  $B \cap C = \emptyset$ , we have

$$\begin{aligned} \delta(A, C) + \delta(B, C) &= \delta(A, A \cap C) \vee \delta(C, A \cap C) + |B| \vee |C|, \\ &= (|A| \vee |C| - |A \cap C|) + |B| \vee |C|, \\ &= |A| \vee |C| + (|B| \vee |C| - |A \cap C|), \\ &\geq \delta(A, B), \end{aligned}$$

where the inequality follows from  $|B| \vee |C| \geq |C| \geq |A \cap C|$  and  $\delta(A, B) = |A|$ . Now, assume  $A \cap C \neq \emptyset$  and  $B \cap C \neq \emptyset$ . Observe that

$$\begin{aligned} \delta(A, C) + \delta(B, C) &= \delta(A, A \cap C) \vee \delta(C, A \cap C) \\ &\quad + \delta(B, B \cap C) \vee \delta(C, B \cap C) \\ &= (|A| \vee |C| - |A \cap C|) + (|B| \vee |C| - |B \cap C|), \\ &= (|A| \vee |C| + |B| \vee |C|) - (|C \cap A| + |C \cap B|), \\ &\geq |A| \vee |C| + (|B| \vee |C| - |C|) \\ &\geq \delta(A, B), \end{aligned}$$

where the second inequality follows from the fact that  $(C \cap A)$  and  $(C \cap B)$  are mutually exclusive subsets of  $C$ . The proof of the last case where  $A \cap B \neq \emptyset$  and  $B$  is not a subset of  $A$  is almost the same as the second case, and hence we do not include it here.  $\square$

With a valid metric  $\delta$ , we can define a neighborhood of a given  $A \in \Omega$ :

$$\mathcal{N}_\xi(A) = \{B \in \Omega : \delta(A, B) \leq \xi \text{ where } \xi \in \mathbb{R}^+\}.$$

Now we are ready to state the main result of this study.

**Theorem 2.2** Let  $(S_1^{Pr}, S_2^{Pr})$  denote a solution obtained by the proposed method. Then,  $(S_1^{Pr}, S_2^{Pr})$  is at least a local minimum in that there exists some  $\xi_* > 0$  such that for all  $S_1^* \in \mathcal{N}_{\xi_*}(S_1^{Pr})$ ,

$$\mathcal{L}(S_1^{Pr}, S_2^{Pr}) - \mathcal{L}(S_1^*, S_2^*) \leq 0,$$

where  $S_2^* := S \setminus S_1^*$ .

**Proof.** To conserve a space, let  $\mathcal{L}^*$  and  $\mathcal{L}^{Pr}$  denote  $\mathcal{L}(S_1^*, S_2^*)$  and  $\mathcal{L}(S_1^{Pr}, S_2^{Pr})$ , respectively. When  $S_1^* \in \mathcal{N}_{\xi_*}(S_1^{Pr})$ , one of the followings should hold; (i)  $S_1^* \subset S_1^{Pr}$ ; (ii)  $S_1^* \supset S_1^{Pr}$ ; and (iii) neither of (i) nor (ii) is true. We shall show that the claim holds true for all the cases. To begin with, consider the first case and assume that there exists some  $S_1^*$  such that  $\mathcal{L}^* - \mathcal{L}^{Pr} < 0$ . Let  $\xi_1 := |S_1^{Pr}| - 1$ . Note that  $S_1^* \in \mathcal{N}_{\xi_1}(S_1^{Pr})$ . Let  $S_1^{Pr} \setminus S_1^* := \{\mathbf{w}_1, \dots, \mathbf{w}_{C_1}\}$ . Then difference of  $\mathcal{L}^*$  and  $\mathcal{L}^{Pr}$  can be rewritten as

$$\mathcal{L}^* - \mathcal{L}^{Pr} = NG(\mathbf{w}_1; S_1^{Pr}) + \sum_{i=2}^{C_1} NG(\mathbf{w}_i; S_1^{Pr} \setminus \cup_{j=1}^{i-1} \{\mathbf{w}_j\})$$

First,  $NG(\mathbf{w}_1; S_1^{Pr})$  should be greater than or equal to 0; otherwise,  $\mathbf{w}_1 \in \mathcal{T}(S_1^{Pr})$ , which contradicts the stopping criterion of the proposed algorithm. For the rest of netgains, there should be some  $2 \leq i_* \leq C_1$  such that

$$NG(\mathbf{w}_{i_*}; S_1^{Pr} \setminus \{\mathbf{w}_1, \dots, \mathbf{w}_{i_*-1}\}) < 0,$$

not to violate  $\mathcal{L}^* < \mathcal{L}^{Pr}$ . Then, recursive application of Lemma 2.1 will, in turn, yield  $NG(\mathbf{w}_{i_*}; S_1^{Pr}) < 0$ , which again contradicts the stopping criterion of the proposed algorithm. Consequently, there can not exist any negative netgain, thereby resulting in  $\mathcal{L}^* \geq \mathcal{L}^{Pr}$ , which is a contradiction. For the case that  $S_1^* \supset S_1^{Pr}$ , the same argument can be applied; only difference between the first and second cases is we transfer some elements from  $S_2^{Pr}$  to  $S_1^{Pr}$ , and hence, we replace  $S_1^{Pr}$  with  $S_2^{Pr}$  in the above argument while  $\xi_1$  will be replaced with  $\xi_2 := |S_2^{Pr}| - 1$ .

Now consider the last case. Let  $A_1$  and  $A_2$  denote  $S_1^{Pr} \cap S_1^* \neq \emptyset$  and  $A_1^c$ , respectively. As in the first case, we have

$$\mathcal{L}(S_1^{Pr}, S_2^{Pr}) - \mathcal{L}(A_1, A_2) < 0.$$

To complete the proof, it suffices to show that the claim holds for  $\xi_* = 1$ . Before proceeding further, define a function  $\text{sgn} : \mathbb{R} \rightarrow \mathbb{R}$  as follows:

$$\text{sgn}(x) := \begin{cases} 1, & \text{if } x > 0; \\ 0, & \text{if } x = 0; \\ -1, & \text{if } x < 0. \end{cases}$$

In succession, assume that  $S_1^{Pr} = A_1 \cup \{\mathbf{w}_1\}$  and  $S_1^* = A_1 \cup \{\mathbf{v}_1\}$  so that  $\delta(S_1^*, S_1^{Pr}) = 1$  but  $S_1^* \cap S_1^{Pr} \neq \emptyset$ . Note that  $A_2 = S_2^{Pr} \cup \{\mathbf{w}_1\}$ , i.e.,  $S_{Pr}^2 = A_2^{-\{\mathbf{w}_1\}}$ , and hence, Lemma 2.1 implies

$$\text{sgn}\left[NG(\mathbf{v}_1; A_2)\right] = \text{sgn}\left[NG(\mathbf{v}_1; S_2^{Pr})\right] = 1,$$

where the last equality holds since  $\mathbf{v}_1$  should, otherwise, be transferred to  $S_1^{Pr}$ , which is a violation of the stopping criterion. Note that the last equality also implies

$$(2.8) \quad NG(\mathbf{v}_1; S_2^{Pr}) = \mathcal{L}(A_1, A_2) - \mathcal{L}(S_1^{Pr}, S_2^{Pr}) > 0.$$

On the contrary,  $S_1^* = A_1 \cup \{\mathbf{v}_1\}$  and  $A_2 = S_2^* \cup \{\mathbf{v}_1\}$ , and hence

$$NG(\mathbf{v}_1; A_2) = \mathcal{L}(S_1^*, S_2^*) - \mathcal{L}(A_1, A_2) > 0.$$

Consequently, (2.8) implies that

$$\mathcal{L}(S_1^{Pr}, S_2^{Pr}) < \mathcal{L}(A_1, A_2) < \mathcal{L}(S_1^{P*}, S_2^{P*}),$$

which completes the proof of the theorem. □

Next paragraph describes how the distance function behaves on the given domain in the case of  $K = 2$ . To that end, we shall define a sequence of pairs of sets  $(S_1, S_2)$ . Recall  $S_1 = \{\mathbf{s}_1^1, \mathbf{s}_2^1, \dots, \mathbf{s}_{n_1}^1\}$  and  $S_2 = \{\mathbf{s}_1^2, \mathbf{s}_2^2, \dots, \mathbf{s}_{n_2}^2\}$ . Note that  $S_2 = S \setminus S_1$ . Define  $T_1^1 := S_1^{(+n_2)} = S_1 \cup \{\mathbf{s}_{n_2}^2\}$ , that is, the  $n_2$ th element of  $S_2$  will be transferred from  $S_2$  to  $S_1$ . Next, let  $T_2^1$  denote the complement of  $T_1^1$ , that is,  $T_2^1 := S \setminus T_1^1$ . Therefore, numbers of elements in  $T_1^1$  and  $T_2^1$  are  $n_1 + 1$  and  $n_2 - 1$ , respectively. Recursively, define

$$\begin{aligned} T_1^2 &= T_1^{1, (+n_2-1)} = S_1 \cup \{\mathbf{s}_{n_2-1}^2, \mathbf{s}_{n_2}^2\} \\ T_2^2 &= S - T_1^2 = S_2 - \{\mathbf{s}_{n_2-1}^2, \mathbf{s}_{n_2}^2\} \\ &\vdots \\ T_1^{n_2} &= T_1^{(n_2-1), (+1)} = S_1 \cup \{\mathbf{s}_1^2, \dots, \mathbf{s}_{n_2-1}^2, \mathbf{s}_{n_2}^2\} \\ T_2^{n_2} &= S - T_1^{n_2} = S_2 - \{\mathbf{s}_1^2, \dots, \mathbf{s}_{n_2-1}^2, \mathbf{s}_{n_2}^2\}. \end{aligned}$$

Note that the superscript denotes the ordinal number of stage which implies that number of elements are moved from  $S_2$  to  $S_1$ . It is plain to see that  $T_1^{n_2} \equiv S$  and  $T_2^{n_2} \equiv \emptyset$ . Next, we

define a sequence of sets in an opposite manner

$$\begin{aligned}
R_1^1 &:= S_1^{(-n_1)} = S_1 - \{\mathbf{s}_{n_1}^1\} \\
R_2^1 &:= S_2^{(+n_1)} = S_2 \cup \{\mathbf{s}_{n_1}^1\} \\
R_1^2 &= R_1^{1,(-n_1-1)} = S_1 - \{\mathbf{s}_{n_1-1}^1, \mathbf{s}_{n_1}^1\} \\
R_2^2 &= S - R_1^2 = S_2 \cup \{\mathbf{s}_{n_1-1}^1, \mathbf{s}_{n_1}^1\} \\
&\vdots \\
R_1^{n_1} &= R_1^{(n_1-1),(-1)} = S_1 - \{\mathbf{s}_1^1, \dots, \mathbf{s}_{n_1-1}^1, \mathbf{s}_{n_1}^1\} \\
R_2^{n_1} &= S - R_1^{n_1} = S_2 - \{\mathbf{s}_1^1, \dots, \mathbf{s}_{n_1-1}^1, \mathbf{s}_{n_1}^1\}
\end{aligned}$$

where  $R_1^{n_1} = \emptyset$  and  $R_2^{n_1} = S$ . Finally, we have

$$\emptyset = R_1^{n_1} \subset \dots \subset R_1^1 \subset S_1 \subset T_1^1 \subset \dots \subset T_1^{n_2} = S$$

and

$$S = R_2^{n_1} \supset \dots \supset R_2^1 \supset S_2 \supset T_2^1 \supset \dots \supset T_2^{n_2} = \emptyset$$

Define a collection of pairs of sets as follows

$$\mathcal{T} := \{(R_1^{n_1}, R_2^{n_1}), \dots, (R_1^1, R_2^1), (S_1, S_2), (T_1^1, T_2^1), \dots, (T_1^{n_2}, T_2^{n_2})\}.$$

Note that  $\mathcal{T} \subset \mathcal{S}^2$ .

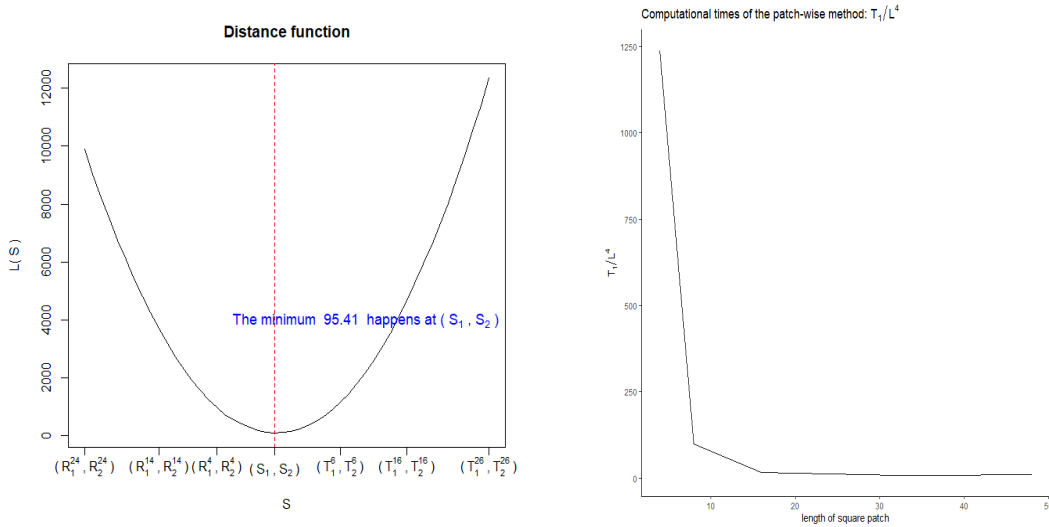


Figure 2: A graph of  $\mathcal{L}$  over  $\mathcal{T}$  (left) and computational runtime (right)

**Example 2.** Recall the images from Example 1. Let  $S_1$  and  $S_2$  denote sets of pixels which belong to the white circle and black area, respectively. Without a noise, the segmentation

of the white circle  $S_1$  is not challenging at all. Even though the noise in this example is not strong enough to make the segmentation challenging, the presence of stronger noise adds more difficulty than would otherwise be the case. With the real observed image with a noise, the segmentation of the white circle amounts to specifying locations of pixels belonging to  $S_1$ , that is, estimating  $S_1$ . Figure 2 shows a graph of the distance function over  $\mathcal{T}$ . As displayed in the figure,  $\mathcal{L}$  attains the minimum at  $(S_1, S_2)$ , the true locations of the white circle and black area. Therefore, solving optimization problem of the CvM distance function – which is defined in (2.3) – indeed yields good estimates  $\widehat{S}_1$  and  $\widehat{S}_2$ .

### 3 Simulation studies

#### 3.1 General setup

Recall the model (2.1). Through this section, we use a collection of pixels

$$S = \{(i, j) : 1 \leq i \leq 200, 1 \leq j \leq 200\},$$

i.e.,  $S$  is a  $200 \times 200$  square. As Example 1, we consider  $K = 2$  and assume that  $g : \mathbb{R}^2 \rightarrow \mathbb{R}$  takes  $p_1 = 1$  and  $p_2 = 0$  over  $S_1$  and  $S_2$ , respectively. For the error in the model (2.1), we assume that it follows a normal distribution with mean of zero and standard deviation of  $\sigma$ . For the comparison purpose, several values will be tried for  $\sigma = 0.1, 0.5,$  and  $0.8$ , which are referred to as mild, moderate, and severe errors, respectively. Kim [5], [6] showed that the minimum distance estimators of linear models with both independent and dependent errors – which follow a wide range of distributions, including a normal, logistic, Cauchy, and mixture of two distributions – outperform other estimators such as maximum likelihood, the least squares, several M-estimators (Huber, Tukey bisquare, and least median squares). However, we report the simulation result corresponding to the normal error only; result corresponding to other errors will be available on the request. For the computational simulation in this study, RStudio 1.1.463 is used; the CPU used for gauging the computational speed is Intel(R) Core(TM) i7-10700.

Note that the size of all images used for the simulation studies is  $200 \times 200$ . Segmentation of  $S_1$  from a  $200 \times 200$  image is not computationally expensive in that it does not take much time. However, some real images – e.g., magnetic resonance images – of a large dimension will take quite substantial amount of time. Therefore, it is absolutely imperative to address ensuing issues after considering the segmentation of  $S_1$  from a larger image, that is, computational cost. To this end, next section will make a breakthrough in the expensive computational cost: patch-wise segmentation.



### 3.2 Patch-wise segmentation

To establish the superiority of the patch-wise segmentation over the traditional segmentation method without using patch images, we will demonstrate that segmentation can be implemented much faster through the patch-wise method, which is not attainable through the full segmentation. For the input image for the segmentation, we will use the cross image with error of  $\sigma = 0.5$  in Figure 5. To assess how the patch size affects the computational time of the segmentation, various square patch images whose lengths range between 4 and 48 will be tried. For each square patch, we will repeat the segmentation 100 times, measure the time taken by whole iterations, and record the total time divided by 100 as the final computational time. The table below reports the results of the patch-wise segmentation corresponding to the various patch sizes. Note that the size of the input image is  $200 \times 200$ . The first column

$L$ (length)	$T$ (seconds)	$N$ (# of patches)	$T_1$ ( $\times 10^{-5}$ )	$T_1/L$	$T_1/L^2$	$T_1/L^3$ ( $\times 10^{-3}$ )	$T_1/L^4$ ( $\times 10^{-2}$ )
4	3.104	9801	316.702	79.176	19.794	494.847	1237.119
8	3.804	9409	404.294	50.537	6.317	78.964	98.705
16	9.562	8649	1105.561	69.098	4.319	26.991	16.87
32	65.622	7225	9082.63	283.832	8.87	27.718	8.662
36	103.492	6889	15022.79	417.3	11.592	32.199	8.944
40	156.108	6561	23793.324	594.833	14.871	37.177	9.294
44	233.756	6241	37454.895	851.248	19.347	43.969	9.993
48	323.786	5929	54610.558	1137.72	23.702	49.38	10.288

Table 1: Computational times when patch images of various sizes are used.

denoted by  $L$  represents the length of the square patch used for the segmentation while the second column denoted by  $T$  reports the final computational time taken by the segmentation when the square patch of corresponding length is used. For example, using a square patch of length 32 requires 65.622 seconds for the segmentation of the entire  $200 \times 200$  input image while only 3.804 seconds is taken for the same segmentation when a square patch of length 8 is used.

The third column denoted by  $N$  represents the number of extracted patch images during the entire segmentation. Since a stride of 2 is used when a square patch slides for both horizontal and vertical ways,  $N$  is equivalent to  $[(200 - L)/2 + 1]^2$ .  $T_1$  in the fourth column denotes  $T/N$  which is average time taken for segmentation of a single square patch where the figure in the parenthesis is a unit of computational time. For example, it will take  $404.294 \times 10^{-5}$  seconds on average for the segmentation of an  $8 \times 8$  image. From the fifth to the last columns,  $T_1$  divided by  $L^k$  with  $k = 1, 2, 3, 4$  are reported.  $T_1/L^k$  with  $k = 1, 2, 3$  increase as  $L$  increases while the opposite result holds for  $k = 4$ . When  $k = 4$ ,  $T_1/L^4$  initially decreases. Once  $L$  reaches 32, it is stabilized around  $10 \times 10^{-2}$ , which implies the

computational time ( $T_1$ ) of a  $L \times L$  square image is approximately proportional to  $L$  raised to 4th power. Figure 2 (right) displays the relationship between  $T_1/L^k$  and  $L$ , which again corroborates our findings. In what follows, the patch-wise segmentation will be used for the analysis unless specified otherwise.

### 3.3 Image segmentation of simulated images

We shall generate various simulated images such as circle, square, triangle, and star. Upon generating those images, we apply the proposed method to separate the white regions from the entire image. To visualize performance of the proposed method, we invert the colors of the resulting images after the segmentation, that is, transforming white pixels to black pixels or vice versa. Figures 3-6 show original images together with their segmented outputs: Figure 3 shows the result pertaining to the original image without noise while Figures 4, 5, and 6 show the results when the original image with noise generated from a normal distribution with  $\sigma=0.1, 0.5,$  and  $0.8,$  respectively.

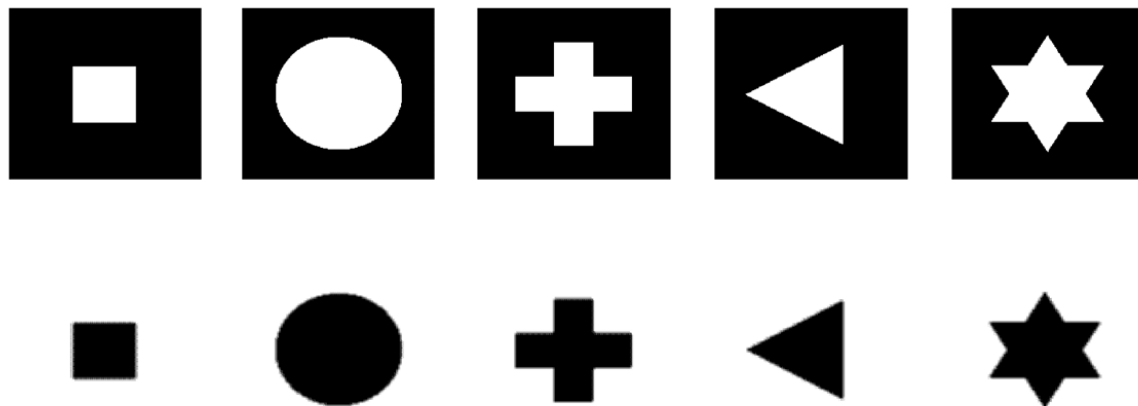


Figure 3: Original images (top) and segmented images (bottom)

A several points are worth mentioning here. First, the proposed method returns perfect segmented images when there is no error (Figure 3) or mild error. Even in the presence of moderate error, the proposed method show very good segmentation performance; there are only few false-positively segmented pixels which do not belong to  $S_1$  but are wrongly segmented. These false-positively segmented pixels are often described using the umbrella term, "noise," in the literature. Note that number of noises in the final segmented image increases when images contain severe errors as shown in Figure 6. Secondly, it is clear to see the border lines between  $S_1$  (white) and  $S_2$  (black) get blurred as the error gets stronger ( $\sigma$  increases), thereby becoming a serious impediment to the accurate segmentation. A closer

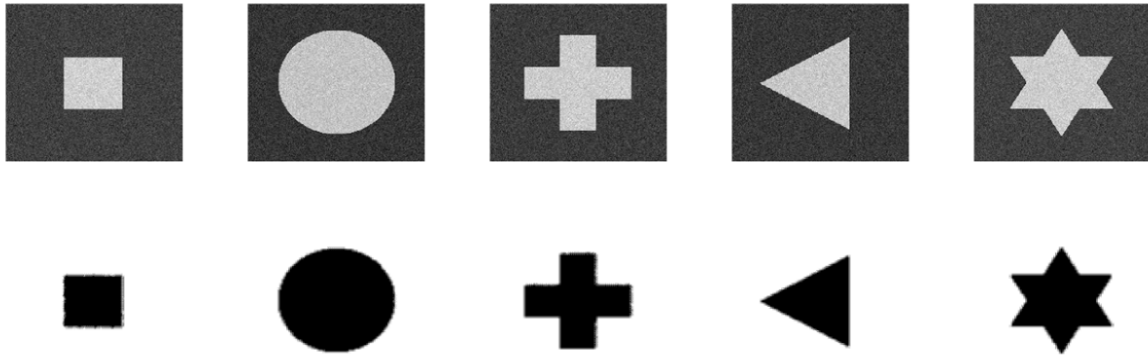


Figure 4: Original images with mild errors (top) and segmented images (bottom)

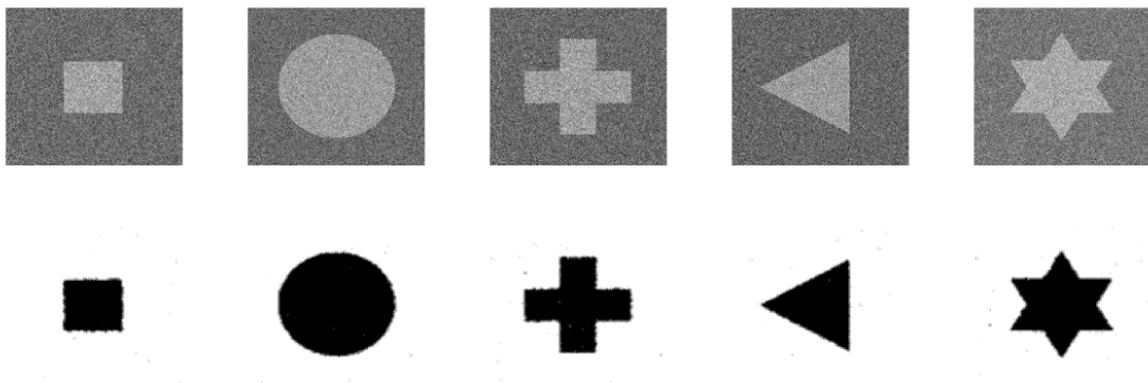


Figure 5: Original images with moderate errors (top) and segmented images (bottom).

look at the images with severe errors will reveal that the border lines of the segmented images are not straight but all saw-edged. In an effort to reduce (or remove completely if possible) noise, we integrate the patch-wise segmentation with a digital filtering technique such as patch-wise segmentation and median filter which are popular and widely used in digital image processing for their several merits: see, e.g., Huang et. al [4] for more details. Figure 7 shows results of the patch-wise segmentation with or without the median filtering. As shown in the figure, it is crystal-clear that there is a stark difference between two figures: most of the noises are removed when the median filtering is applied.

As shown in the figure, the proposed method perform the image segmentation well for all cases. Considering the complexity of usual real images (e.g., a cat, dog, etc), the result in the figure, however, is not motivating. To substantiate the proposed method has a potential real-world application, we try a more complicating image: a  $100 \times 100$  psuedo-QR code image

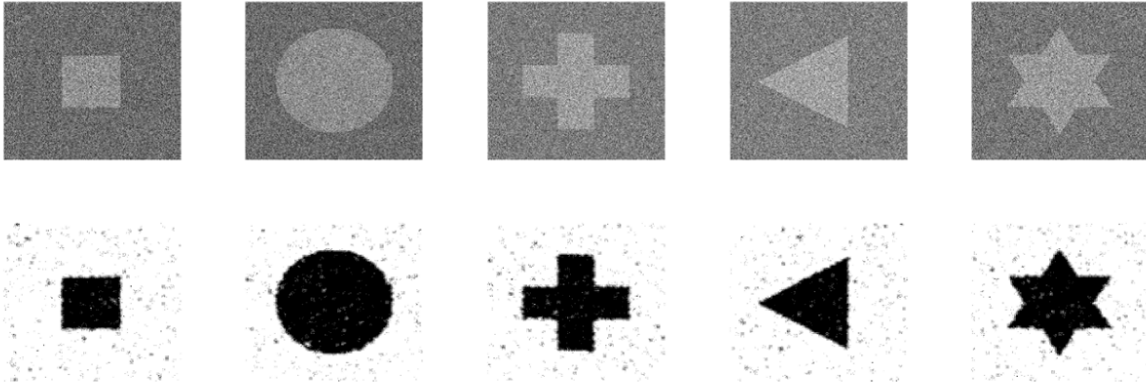


Figure 6: Original images with severe errors (top) and segmented images (bottom).



Figure 7: Segmented image without (left) and with (right) the median filtering.

which resembles a QR code but is a fake image. For generating the QR image, we obtain 5,000 pairs of  $(i, j)$ 's by randomly generating  $i$  and  $j$  from the discrete uniform distribution on  $\{1, 2, \dots, 100\}$  and assign 1 to the  $(i, j)$ th entry of the image for the pixel value while 0 will be assigned to the rest entries of the image. Therefore, the resulting image will contain the same number of white and black pixels. Figure 8 reports the result pertaining to a psuedo-QR code image.

Even just a quick glance reveals that the performance of the proposed method deteriorates to a large extent when being compared with the previous cases of the simple images. One point worth noting at this juncture is that the full-fledged error is not even introduced yet in the image. The competence to handle the presence of errors and a complexity of a target image is an indispensable virtue that the proposed method should have in order to remain as a competitive method for the image segmentation. Otherwise, application of the proposed method to a image segmentation task is merely reinventing the wheel.



Figure 8: The original pseudo-QR image (left) and segmented image (right)

### 3.4 Segmenting-together-strategy

As shown in the QR image case, the proposed method displayed a disappointing performance. To redress this issue, we propose a novel strategy as an addendum to the proposed method: we refer to this strategy as “segmenting-together-strategy”, which implies, ad litteram, segmenting a group of similar pixels together rather than a disparate group of pixels. Figure 9 describes the general procedure of the segmenting-together strategy when it is applied to an  $4 \times 5$  image. The procedure consists of three stages; (1) transforming the original image;

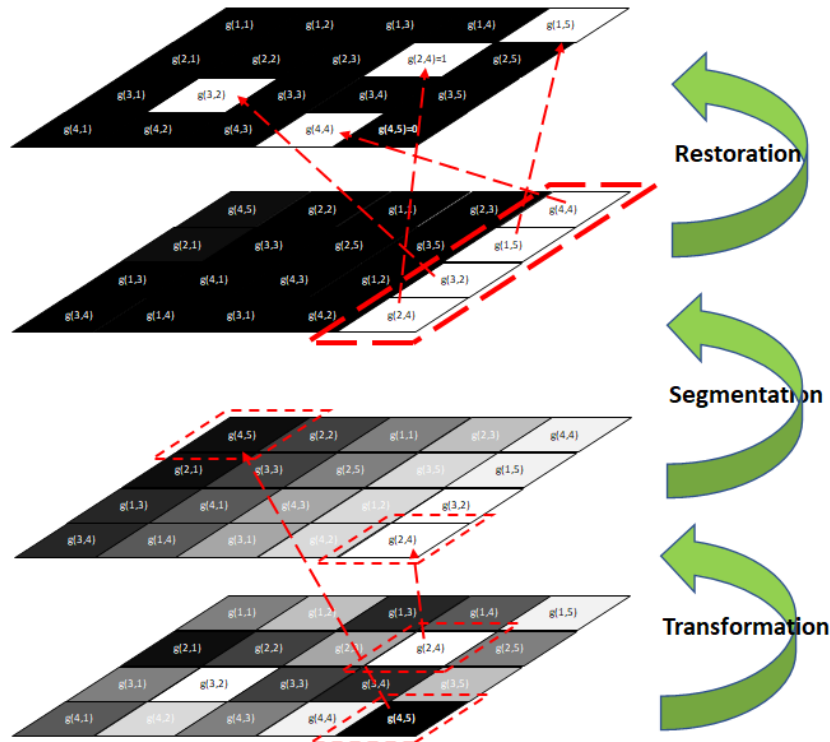


Figure 9: Transformation and retrieval of an image through sorting pixels: an original image(bottom), a transformed image(middle) and a retrieved image.

(2) segmenting the cluster of bright pixels; and (3) restoring the segmented pixels to their original entries. In the stage of transformation, pixels will be sorted and arranged in an increasing order of pixel values; the (4,5)th entry, as a case in point, of the original image having the least pixel value (=0) will be relocated to the (1,1)th entry of the transformed image while the (2,4)th entry of the original image with the largest pixel value of 1 will be relocated to the (4,5)th entry of the transformed image. For the transformation of any  $M \times N$  image, we can define an associated one-to-one mapping  $\phi : \mathbb{N} \times \mathbb{N} \rightarrow \mathbb{N} \times \mathbb{N}$ , that is,

$$\phi(i_2, j_2) = (i_1, j_1), \quad 1 \leq i_1, i_2 \leq M, \quad 1 \leq j_1, j_2 \leq N,$$

where  $(i_1, j_1)$  represents the  $(i_1, j_1)$ th entry of the original image while  $(i_2, j_2)$  represents the  $(i_2, j_2)$ th entry of the transformed image. Through referring to  $\phi$ , we can ascertain an original entry of a given entry of the transformed image, and hence, the original entry of any entry of the transformed image can be retrieved in any time. In the original image of the figure, let the four brightest pixels – the (1,5)th, (2,4)th, (3,2)th, and (4,4)th entries of the image – constitute a region of interest (ROI). After the transformation, these pixels will be relocated to the last column of the new image. Upon the completion of transforming the original image, we apply the proposed method to the resulting image for the segmentation. Assume that only those four pixels of ROI survive an segmentation process while others do not. Then, we highlight those survived pixels by changing their pixel values to 1 while transforming other pixels completely black by assigning 0 for the pixel value. Finally, those segmented pixels will be restored to their original entries by referring to the mapping  $\phi$ .

Figure 10 compares outcomes obtained from the proposed method only (middle) and the proposed method in conjunction with the segmenting-together-strategy (right). From the

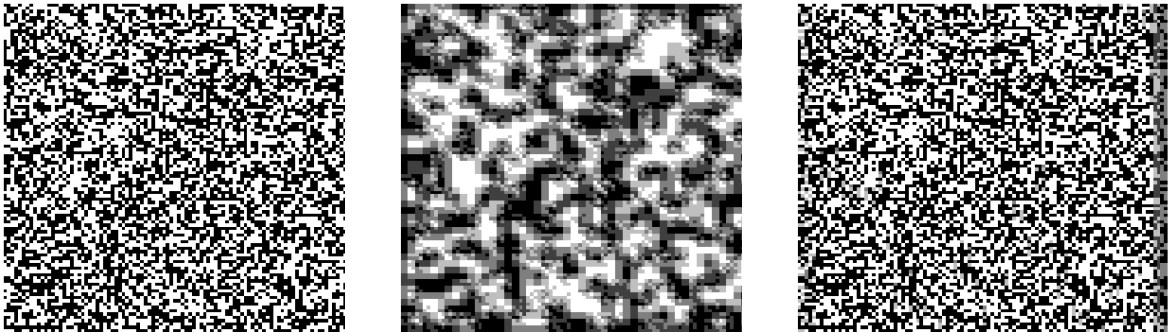


Figure 10: Original QR images (left), segmented image by the proposed method (middle) and image by the proposed method together with segmenting-together strategy (right).

figure, it is immediately apparent that the proposed method shows a remarkable improvement

in performance when combined with the segmenting-together-strategy, thereby indirectly proving the preponderant role of the strategy. This becomes clear when we investigate the outcome obtained from the proposed method with the strategy in greater detail. To this end, we first invert the segmented image, superimpose it on the original image, and examine how much the overlaid image fills the original image. If the segmentation is perfect, then the resulting image will be completely black; on the contrary, the resulting image will be the original image itself if the segmentation goes completely awry; otherwise, the resulting image will range from the original image to a complete black image, *pari passu* to the performance of the proposed method. Figure 11 reports the result of the overlay analysis. As reported

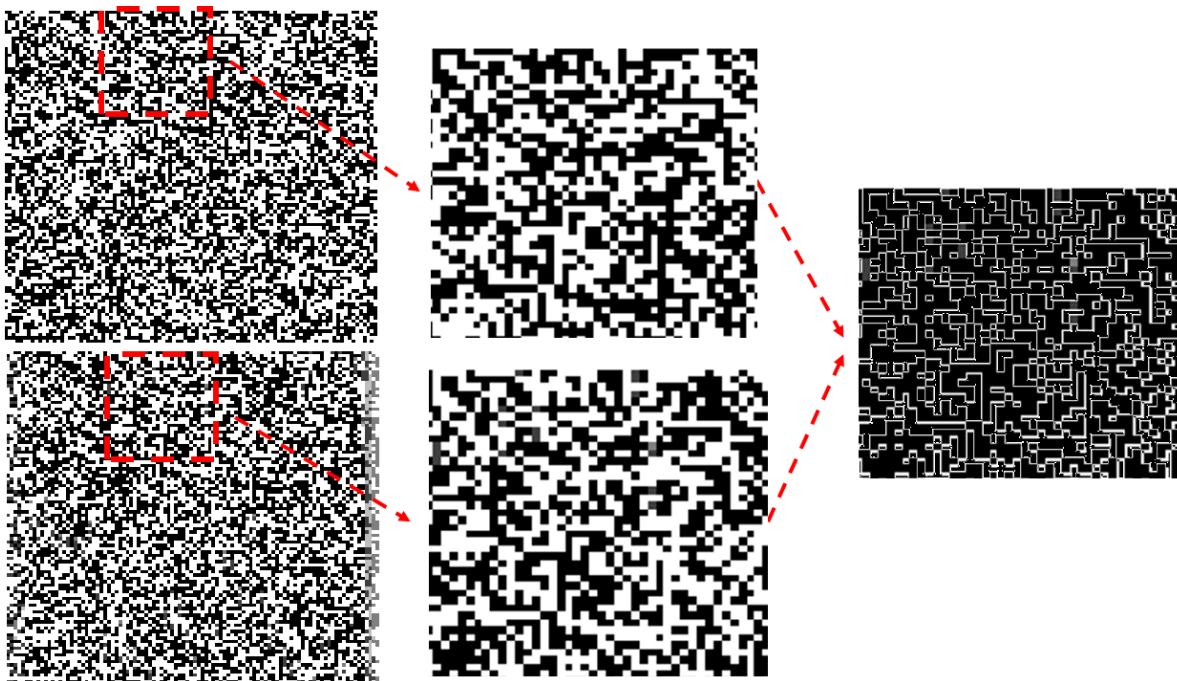


Figure 11: Comparison of the original image and the resulting image from the segmenting-together-strategy.

in the figure, the overlaid image almost perfectly fills the original image, and hence, the resulting image is almost black. To delineate the exquisite performance of the proposed method with the strategy when compared with the proposed method only, we will employ another measure which gauges the similarity between the original image and the segmented image: Dice similarity coefficient (DSC) which is defined as

$$DSC = \frac{2|A \cap B|}{|A| + |B|},$$

for given two images  $A$  and  $B$  where  $|\cdot|$  implies the cardinality of a image, that is, the number of pixels in a image. The DSC value of the segmented image from the proposed

method only (middle of Figure 10) is 0.625, which implies it correctly matches only 62.5% of the entire original image. When the proposed method is combined with the segmenting-together-strategy, the DSC surges to 0.942, thereby showing drastic improvement. Figure

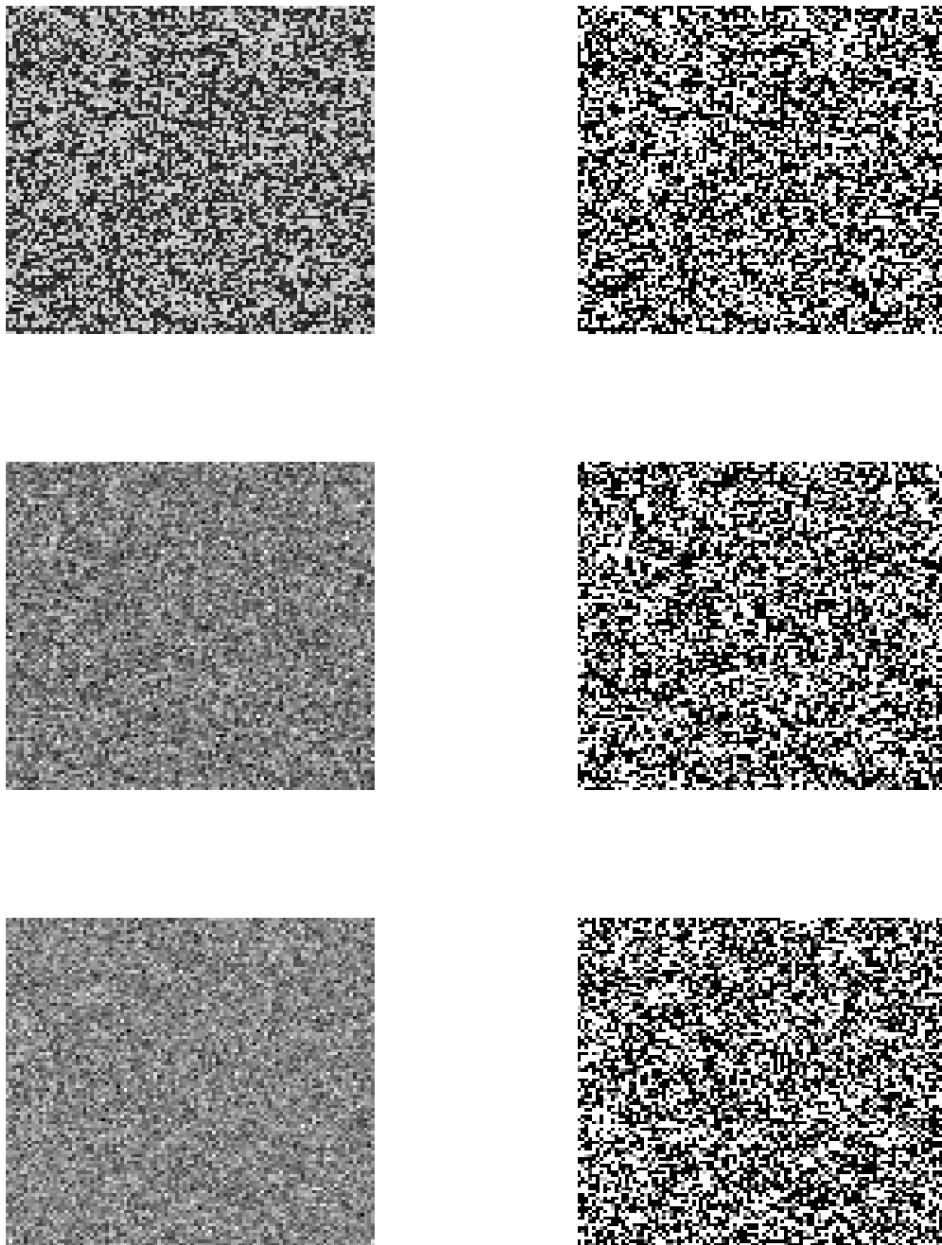


Figure 12: Original QR images with various errors (left) and segmented images (right).

12 reports the segmentation results (right) when the QR images (left) contaminated by various errors are segmented through the proposed method with the strategy: mild (top),



moderate (middle), and severe (bottom) errors, respectively. Then, we obtain the DSC values of 0.931, 0.798, and 0.707 for the mild, moderate, and severe errors, respectively. Recall the case of the QR image without any errors where the proposed method only yielded the DSC value of 0.625. When the proposed method is combined with the strategy, it yields still better performance in terms of the DSC value even in the presence of the severe errors. This finding also closely accords with robust features of MD estimation method which were described in the introduction of this article.

### 3.5 Real examples

The previous section observed that the felicitous conjunction of the proposed method and the segmenting-together-strategy came as an amazement. However, the results obtained from the simulation studies in the previous section should be treated and interpreted with considerable caution. It is not surprising to frequently observe that excellence of methods with the simulated data are belied by the poor performance in real data: they starts brilliantly with the simulated data but sink into or below mediocrity with real data. At this juncture, we have to answer the following question: can the proposed method replicate the theoretical result obtained so far when it is applied to the real data? Successful replication will lend credence to the proposed method while failure to do that will cast a pall of suspicion over the method. In view of this, showing good performance is crucial. To this end, this section; (1) assesses the performance of the proposed method when the real data is used for the segmentation; and (2) demonstrates that the proposed method will remain competitive even when it is adopted for handling real data, thereby consolidating its position as the potential option for the image segmentation.

For the real data, we use the magnetic resonance (MR) images of brain tumors from Baid et al. [1]. In the MR images of brain, the tumors are denoted by bright colors while normal cells are denoted by dark colors. In the gray-scale MR images, tumors have a pixel value of or close to 1 (white) while normal cells have a pixel value of or close to 0 (black). Figures 13 and 14 report the result when the proposed method together with the segmenting-together-strategy is employed for different types of two MR images: Fluid-attenuated inversion recovery (FLAIR) and T1-weighted images. Figure Fig:RSNA1 shows the original flair MR image (left), the inverted image of the segmentation (middle) and the overlay of segmented image over the original one (right). Based on the overlay of the segmented image, the proposed method seems to work properly: it is, at least, not a meretricious method which works for the simulated data only. As shown in the segmented image, there are still some false positives; however, most of all of those are located in the area of the skull which of the original image is denoted by as much bright pixels as tumors. During preparing the MR image before the segmentation – which is called “preprocessing” – those bright pixels in the skull are removed.

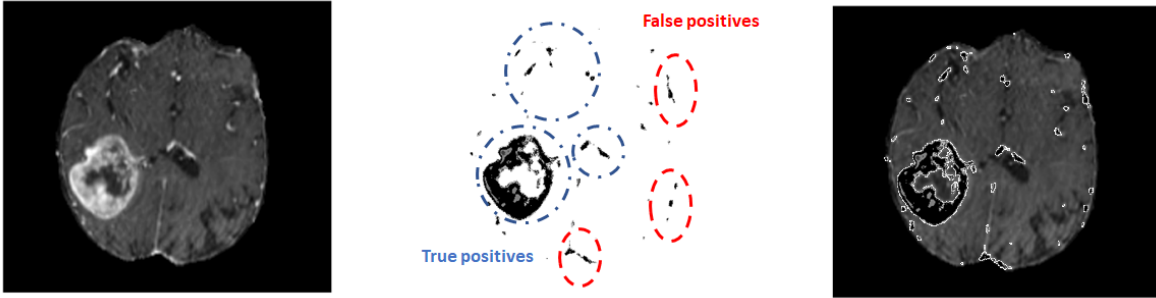


Figure 13: A FLAIR image of brain tumors (left), the segmented image by the proposed method (middle), and the overlaid image (right)

Therefore, those false positives might be imputed to the less careful preprocessing procedure of the MR image. If the better-preprocessed image were used, then those types of false positives would disappear. One promising fact here is that the proposed method successfully detect tumors of a very small size which are located inside of the top blue circle in the middle image: we surmise that this finding is originated from the segmenting-together-strategy. Without it, those small tumors could have not been detected. This finding adds cachet to the extant desirable features of the MDE method such as robustness. Figure 14 reports a

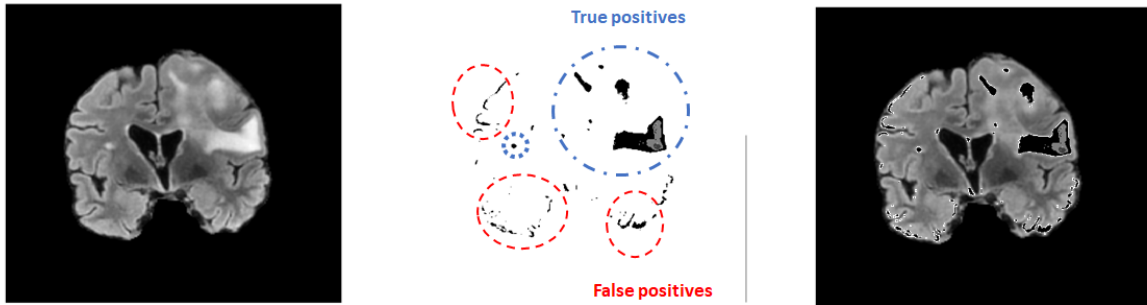


Figure 14: A T1-weighted image of a brain cancer (left), the segmented image by the proposed method (middle), and the overlaid image (right)

T1-weighted MR image of different brain tumors. The most striking difference between the T1-weighted and FLAIR images is that the white matter (WM) which is the exterior part inside of the skull is very bright – but still less bright than tumors – in the T1-weighted MR image while it is dark gray, thereby pixels of the WM being close to 0. Therefore, the existence of the WM in the T1-weighted MR image tends to consign successful segmentation of tumors only to a more challenging problem. This is why the FLAIR image is more preferred for the segmentation. As already noticed, the T1-weighted image in Figure 14 shows more false positives. A point worth noting here is that the proposed method successfully

segmented the tumor only – which is in the small blue circle in the middle figure – even in the presence of the WM; this closely accords with the fact that the WM is less bright than the tumor, thereby being ignored by the proposed method. Even though the performance of the image segmentation deteriorated in the T1-weighted image, this issue can be easily resolved in that both the T1-weighted and FLAIR images from the same patient are tried for the segmentation of tumors, and hence, only commonly segmented images are used for detecting tumors. During this process, the issue of the false positive error due to the WM can be alleviated to a great extent. There are other types of MR images such as T2-weighted and quantitative susceptibility mapping (QSM) images. Using the T2-weighted and QSM images together will further enhance the performance of the proposed method.

## 4 Conclusion

This paper demonstrates the MD estimation methodology is versatile in that it can be applied to the image segmentation problems, thereby extending its domain of application from the traditional statistical problems to the applied problems. This paper confines the investigation to the case of  $K = 2$  only, i.e., there exist two regions ( $S_1$  and  $S_2$ ) to segment. Investigation of the case of  $K \geq 3$  will be extension of findings in this study and form future research.

## References

- [1] Ujjwal Baid, Satyam Ghodasara, Suyash Mohan, Michel Bilello, Evan Calabrese, Errol Colak, Keyvan Farahani, Jayashree Kalpathy-Cramer, Felipe C Kitamura, Sarthak Pati, Luciano M Prevedello, Jeffrey D Rudie, Chiharu Sako, Russell T Shinohara, Timothy Bergquist, Rong Chai, James Eddy, Julia Elliott, Walter Reade, Thomas Schaffter, Thomas Yu, Jiaxin Zheng, Ahmed W Moawad, Luiz Otavio Coelho, Olivia McDonnell, Elka Miller, Fanny E Moron, Mark C Oswood, Robert Y Shih, Loizos Siakallis, Yulia Bronstein, James R Mason, Anthony F Miller, Gagandeep Choudhary, Aanchal Agarwal, Cristina H Besada, Jamal J Derakhshan, Mariana C Diogo, Daniel D Do-Dai, Luciano Farage, John L Go, Mohiuddin Hadi, Virginia B Hill, Michael Iv, David Joyner, Christie Lincoln, Eyal Lotan, Asako Miyakoshi, Mariana Sanchez-Montano, Jaya Nath, Xuan V Nguyen, Manal Nicolas-Jilwan, Kerem Ozturk, Bojan D Petrovic, Chintan Shah, Lubdha M Shah, Manas Sharma, Onur Simsek, Salil Soman, Volodymyr Statsevych, Brent D Weinberg, Robert J Young, Ichiro Ikuta, Amit K Agarwal, Sword C Cambron, Richard Silbergleit, Alexandru Dusoi, Alida A Postma, Laurent Letourneau-Guillon, Gloria J Guzman Perez-Carrillo, Atin Saha, Neetu Soni, Greg Zaharchuk,

- Vahe M Zohrabian, Yingming Chen, Milos M Cekic, Akm Rahman, Juan E Small, Varun Sethi, Christos Davatzikos, John Mongan, Soonmee Cha, Javier Villanueva-Meyer, John B Freymann, Justin S Kirby, Benedikt Wiestler, Priscila Crivellaro, Rivka R Colen, Aikaterini Kotrotsou, Daniel Marcus, Mikhail Milchenko, Arash Nazeri, Hassan Fathallah-Shaykh, Roland Wiest, Andras Jakab, Marc-Andre Weber, Abhishek Mahajan, Bjoern Menze, Adam E Flanders, and Spyridon Bakas. The rsna-asnr-miccai brats 2021 benchmark on brain tumor segmentation and radiogenomic classification. [arXiv.org](https://arxiv.org), 2021.
- [2] D. L Donoho and R. C Liu. The "automatic" robustness of minimum distance functionals. The Annals of statistics, 16(2):552–586, 1988.
- [3] D. L Donoho and R. C Liu. Pathologies of some minimum distance estimators. The Annals of statistics, 16(2):587–608, 1988.
- [4] T Huang, G Yang, and G Tang. A fast two-dimensional median filtering algorithm. IEEE transactions on acoustics, speech, and signal processing, 27(1):13–18, 1979.
- [5] Jiwoong Kim. A fast algorithm for the coordinate-wise minimum distance estimation. Journal of statistical computation and simulation, 88(3):482–497, 2018.
- [6] Jiwoong Kim. Minimum distance estimation in linear regression with strong mixing errors. Communications in statistics. Theory and methods, 49(6):1475–1494, 2020.
- [7] Hira L. Koul. Some convergence theorems for ranks and weighted empirical cumulatives. The Annals of mathematical statistics, 41(5):1768–1773, 1970.
- [8] Hira L. Koul. Minimum distance estimation in linear regression with unknown error distributions. Statistics & probability letters, 3(1):1–8, 1985.
- [9] Hira L. Koul. Minimum distance estimation in multiple linear regression. Sankhya. Series A, 47(1):57–74, 1985.
- [10] Hira L. Koul. Weighted Empirical Processes in Dynamic Nonlinear Models. Lecture Notes in Statistics, 166. Springer New York, New York, NY, 2nd ed. 2002. edition, 2002.
- [11] J. Wolfowitz. Estimation by the minimum distance method. Annals of the Institute of Statistical Mathematics, 5(1):9–23, 1953.
- [12] J. Wolfowitz. Estimation of the components of stochastic structures. Proceedings of the National Academy of Sciences - PNAS, 40(7):602–606, 1954.

- [13] J. Wolfowitz. The minimum distance method. The Annals of mathematical statistics, 28(1):75–88, 1957.